Conference Proceedings

EuroSun 2016
Palma de Mallorca (Spain), 11 - 14 October 2016

# Transversal Temperature Profiles of Two-Phase Stratified Flow in the Receiver Tube of a Solar Linear Concentrator. Simplified Analysis

**Antonio Lecuona-Neumann[1], Maximilian Rosner[2] Rubén Ventas-Garzón[1]**

[1] Dep. Ingeniería Térmica y de Fluidos, Grupo ITEA, Universidad Carlos III de Madrid, Leganés, Madrid (Spain)

[2] Dep. Ingeniería Térmica y de Fluidos, Universidad Carlos III de Madrid, Leganés, Madrid (Spain), ERASMUS student from University of Applied Sciences Technikum Wien

## Abstract

A steady-state analytical-numerical heat conduction model has been developed for the peripheral temperature profile in the wall of a straight receiver tube applicable to either parabolic trough or Fresnel solar collectors using innovative counterflow two-phase flow. It uses the slender 1D fin model of heat conduction along the tube wall periphery, which gives an analytical solution to be coordinated with boundary conditions. Constant heat transfer and solar incident irradiance are assumed on finite angle sectors of the tube periphery. This allows consideration for irradiance inhomogeneities and/or two-phase internal flows.

The model has been applied using parameters representative of medium temperature collectors of innovative design. Inside them, a sliding liquid film is established under the effect of gravity vertically stratifying a liquid/vapor two-phase flow. This flow configuration is considered for direct vapor generators/separators for advanced solar driven absorption machines and power plants.

The results show that for a circular tube with wall thicknesses large enough for withstanding typical pressures the peripheral temperature inhomogeneity is reduced. The inhomogeneity increases in the non-central hours of the day above the inhomogeneity found in the central hours of the day. This is so especially if the liquid film is shallow and for parabolic trough solar collectors.

Keywords: *Solar cooling, receiver tube wall, parabolic trough, Fresnel, Medium temperature solar collector,*

## 1. Introduction

### *1.1 Solar thermal*

Solar heating and cooling (SHC) concept has been established as a current technology but still developing. It is well supported by basic studies, such as (Duffie & Beckman, 1980) among others. Nowadays medium temperature (150 – 250 ºC) solar collectors (MTC) e.g. (Jradi & Riffat, 2012) attract much attention because they enable new solar applications for small to medium scale applications. They offer higher flexibility than fixed geometry low-temperature collectors and enjoy the advances in the technology of high-temperature collectors (HTC) of either parabolic trough or Fresnel type collectors used in large solar power plants.

### *1.2 Absorption and working fluids*

Producing cold with the solar heat is an attractive technology, especially for the synchronicity of sun and cold demand.

Absorption machines consume the heat collected from the sun and work as a thermochemical heat pump, following a thermodynamic cycle. They can work either as chillers or as heaters when respectively the useful effect is evaporating or condensing a refrigerant vapour, the same as in mechanical compression cycles (Herold, et al., 1996).


doi:10.18086/eurosun.2016.04.17 Available at http://proceedings.ises.org

Ammonia as refrigerant offer the possibility of refrigerating even below -20 ºC and much experience has been accumulated on its use. Ammonia is a natural refrigerant, widely accepted in industry for its capability of reducing greenhouse and ozone depletion gasses (Danfoss, 2015). The absorption cycles using this refrigerant need higher temperatures on the driving source than with water as a refrigerant when the working fluid is the solution Water/LiBr. This makes medium temperature solar collectors ideal for application to ammonia absorption cycles.

Currently, ammonia based absorption machines use the mixture Ammonia/Water as working fluid (Wu et al., 2014). Several studies have performed on-the-field performance evaluation driving the machine with heated fluid through MT solar collectors (Wang, et al., 2015).

Machines using Ammonia/Water need a rectification tower to purify the ammonia vapor for reducing minute proportions of water. The mixture Ammonia/Lithium Nitrate ($NH_3/LiNO_3$) does not need this bulky and expensive component, but salt crystallization at the inlet of the absorber is a risk. The absence of water reduces corrosion. Several studies confirm the potential of this working fluid (Ventas et al., 2010). Some operating test results are available (Hernández-Magallanes, et al., 2014). Even pre-industrial prototypes are now operative (Zamora et al., 2014). Ammonia as refrigerant implies pressures in the order of 15 bar in the vapour generator.

The current layout of a solar cooling facility includes: a) an outdoor primary circuit of a heat transfer fluid (HTF) including anti-freeze capability, b) a secondary indoor circuit, typically using water, including a heat storage tank and c) a tertiary circuit of chilled water for cold delivery, (Kalogirou S. , 2004) (Lecuona et al., 2009). A heat rejection circuit is also needed when the machine is not air cooled. This leads to a complex facility and the corresponding high procurement and maintenance costs, frequently requiring professionals for maintenance. Efforts toward improving competitivity seem of value for the dissemination of solar polygeneration technology.

### *1.3 Direct steam production*

Direct steam production has been explored and continues to be explored in large solar power plants, e.g. (Eck, et al., 2003) and (Kalogirou et al., 1997). In solar cooling facilities, this can also be of interest, although there is not much work available on that in the open literature. For direct refrigerant vapour production in an absorption machine one proposal would be that the working fluid slides freely inside an inclined receiver tube along its length, partially filling it, see Fig. 1. Stratified two-phase flow favors vapour separation, as the liquid phase flows falling under gravity effect in the lower part of an inclined tube (angle $\beta$ in Fig. 1) progressively evaporating the refrigerant in a fairly homogeneous way. As a consequence the vapour phase flows upwards in the opposite direction, already separated. In (Lecuona et al., 2016) the details and advantages of this layout are described.

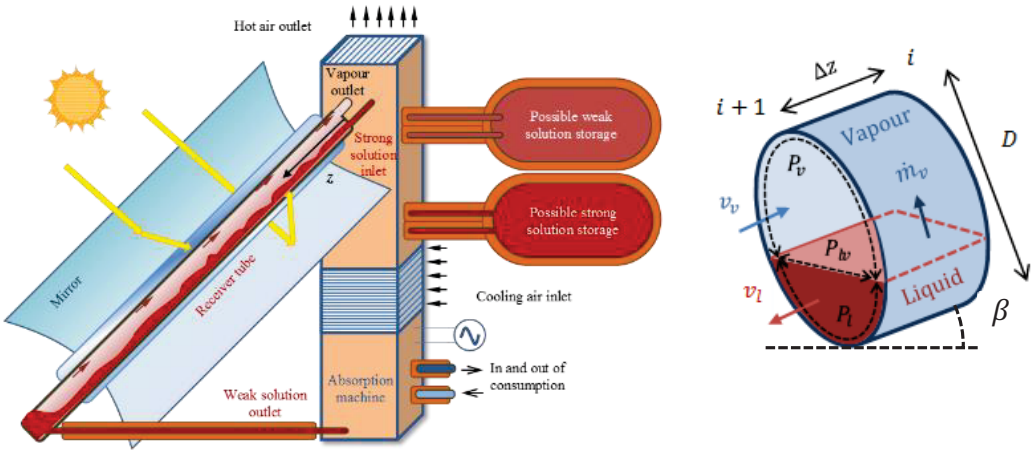

**Fig. 1: Left: Scheme of an elementary solar cooling layout with stratified flow in the receiver tube and attached air cooled absorption machine, eventually incorporating two external storage tanks for energy storage. Right: 1D flow discrete element.**

The higher driving temperature attainable with MTCs allows reaching innovative solar systems using advanced cycles (Ventas et al., 2016). This way, several opportunities appear to reduce the payback period of the solar system and increase coverage of the user demand. As a result cooling capacity can be boosted consuming electricity with the same machine (Vereda et al., 2014). In winter solar direct and/or pumped heat can be produced. Increased *COP* can be attained using double stage/double effect (Ventas et al., 2016). In addition to that production of electricity is possible in periods when neither heat nor cold is needed. The vapors of $NH_3$ are suitable for this purpose as it generates high-pressure differentials between condenser and evaporator of the absorption machine, allowing to easily produce work using expanders or turbines. Small scale MT solar collectors can be built using stationary receiver tubes, thus eliminating the extra cost to avoid $NH_3$ leaks. This is one risk in large format high-temperature parabolic trough solar collectors as they use articulated tubing.

### *1.4 Objectives of the paper*

The receiver tube in linear solar thermal concentrators, such as parabolic trough or Fresnel types, is subjected to bending because of the differential heating between the concentrated sun-irradiated part and the non-irradiated part, typically the upper sector along the tube. This framework can be complicated if a two-phase flow develops inside the tube. Boiling regime is sometimes established when direct steam production is searched for, in conventional solar/electric power plants. This will imply a non-constant peripheral heat transfer to the flow. A higher inhomogeneity develops for a stratified two-phase internal flow. This unconventional flow distribution appears in a novel research area, above described.

There is not much information on the transversal temperature distribution on the wall with this particular flow and irradiation configuration, excepting for other applications, such as (Logie et al., 2015), (Eck et al., 2004), among others. One can expect that when the concentrated solar rays impact on the lower sector of the tube the liquid will evacuate heat at a higher pace that the vapor does in the upper non-irradiated sector of the tube (excepting secondary optics effect). This way there is a compensating effect. In a parabolic trough collector during the morning and afternoon, the sun impacts on the tube laterally so that there is the possibility of overheating as a high irradiance can impact on a vapor flow region. As described in (Lecuona et al., 2016) for the layout described above and schematized in Fig. 1, the vapor can have a lower temperature than the tube wall, but also a higher temperature; thus a practical procedure for calculating the temperature profile around the tube geometry seems useful.

The simulation of the whole solar cooling installation is generally pursued, becoming a complex but accurate model, as complex CFD codes and large computers are required, e. g. (Lobón et al., 2014). Some efforts on simplification are evident (Ahmed, 2014). In order to reduce modeling cost, there is an interest on low order models that keep the relevant physics, thus valid for preliminary studies.

The calculation of the temperature distribution on the wall of the receiver tube is well addressed decomposing the tube wall perimeter in a numerous ensemble of finite elements and applying the combined tangential-radial 2D heat conduction equation, including heat application and/or heat transfer in the radial direction. Axial heat conduction is frequently neglected owing to the much lower temperature gradient in this direction, excepting near brackets. The resolution of a large set of algebraic linear governing equations is performed in a standard way, delivering precise enough temperatures. Reducing the problem to 1D allows considering tangential conduction on top of the radial conduction, thanks to the linearity of the governing equations.

This paper addresses the simplified calculation of the temperature distribution on the periphery of the tube. In order to avoid the excessive computer load of a finite elements calculation, at each axial stage of the tube, the exact 1D analytical solution of the heat conduction equation is invoked. This is typically called the fin approximation (Incropera, De-Witt, 1990). A single explicit algebraic equation is needed for each peripheral segment with constant heat transfer, either toward the ambient or towards the inner fluid and constant irradiance. The fins are each other connected to complete the periphery of the tube. Solving a set of

simultaneous linear equations gives the temperature distribution. This can be done analytically in order to get an explicit overall solution, but excepting the simplest cases, the expression gets too large. Consequently, numerically solving the linear system yields a fast and numerically stable solution.

This paper describes a simplified calculation scheme for the steady-state peripheral distribution of the thickness-wise average temperature in the wall of a receiver tube of a linear solar collector with especial emphasis on MT collectors. The external net irradiance is assumed known as well as the heat transfer coefficients in different perimeters of the internal flow.

### *1.5 Preliminary considerations*

From now on $\langle \quad \rangle$ indicates functional dependence. The longitudinal distribution of temperature $T\langle x\rangle$ by conduction along the length $L$ in extended surface bodies that are geometrically slender $\frac{L}{A^{0.5}} \gg 1$ and thermally slender $\frac{\alpha t}{k} \ll 1$ accepts a 1D analytical approximation for some cross sectional area $A\langle x\rangle$ distributions. Such are pins and fins, not having to be straight, but with central line curvature radius $r_{av} \gg t$ , being $t$ the material thickness. Additional requirements are constant: a) heat conductivity $k$, b) lateral heat transfer coefficient $\alpha$ and c) heat added/generated per unit of lateral area $g$. Although the wall in our case exhibits varying temperature along its periphery it is usual to use a constant average heat transfer coefficient from experimental correlations for a single-phase flow, even in the case of adiabatic portions of the wall. Although under different operational conditions (Yang et al., 2012) indicates low inhomogeneities in the Nusselt number of a collector tube. With this generalized practice, only care must be taken to register the adequate hydraulic and thermal diameters of the cross section and eventually to correct if they are different (Sigalés, 2003) and (Lecuona et al., 2016) among others.

This extended surface theory is much used in basic texts, such as (Incropera & DeWitt, 1990) and with more detail in (Sigalés, 2003), among others. A single ordinary linear differential equation results for the temperature $T$ distribution along the large coordinate $x$:

$$\frac{\mathrm{d}^2 T\langle x\rangle}{\mathrm{d}x^2} - \frac{\alpha P}{kA}\left(T\langle x\rangle - T_\infty\right) + \frac{g}{k} = 0 \qquad \text{(eq.1)}$$

$P$ is the wetted perimeter and $T_\infty$ the unperturbed fluid temperature used for $\alpha$.

This model is used for determining the peripheral wall temperature of the receiver tube, assuming $x = r\phi$, where $\phi$ is the circumpherential central angle, thus neglecting curvature effects besides considering that the inner radius is smaller than the outer radius. A fin is used for every segment of periphery where the conditions are fulfilled, actually constant $\alpha$, $T_\infty$ and $g$. These segments will fulfill the boundary conditions with the neighbor ones in order to complete the full periphery. These boundary conditions fully determine the problem and require the simultaneous resolution of a small number of linear algebraic equations. The peculiarities of our case are:

- There are two temperatures $T_\infty$, for heat transfer: internal $T_i$ for either liquid ($_l$) or vapor ($_v$) and external for losses to ambient $T_e$. Each one has its own heat transfer coefficient, respectively $\alpha_i$ and $\alpha_e$.
- On the external side, there is a concentrated incident solar irradiance, affected by optical losses, determining an equivalent per unit volume heat generation $g$.

This simplification is relevant for larger models, such as of an entire solar collector. In these models ease of use, simplification and speed of calculation are important, not neglecting the stability of the numerical algorithm. In our case of stratified two-phase flow, it serves as a tool for preliminary optimization.

## 2. Numerical model development

The one-dimensional heat transfer for the wall temperature $T$ along the periphery central angle $\phi$ , Fig. 2, is given by reformulating eq. 1 using the internal and external heat transfer coefficients $\alpha_i$ and $\alpha_e$. Wall thickness is $t$ and average receiver tube radius, assumed circular, $r_{av} = r_i + \frac{t}{2}$; $w = \frac{t}{r_i}$:

$$\frac{\mathrm{d}^2T}{\mathrm{d}\phi^2} - m^2T = -T_\mathrm{I};\ m^2 = \frac{r_{av}[\alpha_i+\alpha_e(1+w)]}{kw};\ T_\mathrm{I} = \frac{T_i\alpha_i+(T_e\alpha_e+G_{bT}S)(1+w)}{kw} \quad \text{(eq. 2)}$$

Tilted incident solar irradiance on the aperture of the collector is $G_{bT}$ and $S = Ca_0$ is the number of incident suns on the receiver tube; it is the product of the purposely defined geometric concentration $C = L_{ap}/P_s$ times the total optical efficiency of the solar collector $a_0$. $L_{ap}$ is the mirror(s) aperture width, perpendicular to the axial coordinate $z$. $P_s$ is the total perimeter of the receiver tube radiated; thus in a first approximation the irradiance on the tube is considered constant either concentrated, direct ($C = 1$) or null, see Tab. 1. Extension to more elaborate layouts is straightforward.

There are widely used codes for the calculation of the external heat transfer coefficient $\alpha_e$, e. g. (Forristal, 2003), among others as it the series and parallel composition of radiation, conduction, and combined convection heat transfers. Here a practical way is adopted, needing only commercial information, widely available, without needing to know details of the construction and materials of the collectors.

For a three-term efficiency standard curve of the solar collector, according to (ISO/DIS 9806, 2016), with an estimated overall averaged wall temperature $T_{est}$ and an ambient temperature $T_e$ it follows that under nominal steady-state operating conditions with no wind and no axial incidence, $\alpha_e$ can be estimated as:

$$\alpha_e = \frac{[a_1+a_2(T_{est}-T_e)]L_{ap}}{2\pi r_e} \quad \text{(eq.3)}$$

Further corrections are possible, according to the standard prescriptions.

We assume all parameters in eq. 2 constant, excepting dependent variable $T$ and angle independent variable $\phi$. This makes the differential equation linear non-homogeneous, admitting a well-known analytical solution as the addition of a general exponential solution plus a particular solution $T_{pj}$, Tab. 1. For a generic segment $j$ can be expressed as:

$$T_j\langle\phi\rangle = T_{C1j}e^{m\phi} + T_{C2j}e^{-m\phi} + \underbrace{\frac{(T_e\alpha_e+G_{bT}S)(1+w)}{\alpha_i+\alpha_e(1+w)}}_{T_{pj}} \quad \text{(eq. 4)}$$

The peripheral temperature distribution $T\langle\phi\rangle$ is determined by imposing temperature continuity and energy balance by peripheral conduction at both ends of each peripheral sector using this analytical solution that linearly depends on two boundary constants, actually characteristic temperatures, $T_{C1j}$ and $T_{C2j}$. They are free boundary conditions for segment $j$, Fig. 2. Namely:

$$T_{j-1} = T_j;\ \left.\frac{\mathrm{d}T}{\mathrm{d}\phi}\right|_{j-1} = \left.\frac{\mathrm{d}T}{\mathrm{d}\phi}\right|_{j} \quad \text{(eq. 5)}$$

Fig. 2 represents the application case of a single parabolic trough solar collector in a generic non-symmetrical case, corresponding to an out-of-noon solar position and vertically stratified flow of liquid and vapor, a most challenging stratified regime. The circular periphery is divided into 5 sectors, $j$ = Ia, II, III, IV, Ib, as Fig. 2 depicts. The temperature distribution follows the five equations in Tab. 1.

Unknowns are ten inter-boundary temperatures $T_{cjk}$. The five boundary conditions necessary for determining these unknowns and thus the temperature distribution are indicated in Tab. 2.

## 3. Results and discussion

As the parabolic trough solar collectors incorporate a rotatable mirror for sun tracking, the irradiance can impact on the side of the receiver, suggesting the larger temperature inhomogeneities than with Fresnel type collectors of similar receiver tube layout.

Tab. 3 indicates the chosen common parameters as a base case for the application of the model to some representative cases of a parabolic trough collector, varying remaining parameters. This corresponds to a clear day of the year #100 in Madrid (Spain) corresponding to 10th March of a non-leap year, as some kind of overall year representation. No changes in $\alpha_i$ have been considered for changes in wall temperature $T$ as the bulk and wall temperatures are not dissimilar enough for the low concentrated irradiance on the wall of a MT

solar collector, in the order of $10^4$ W m$^{-2}$.

The first study performed analyzes the effect of variations in the tracking angle $\gamma_M$ along the day around the base case $\gamma_M = 0$ corresponding to solar noon. This implies *ceteris paribus*; meaning this "all other parameter unchanged". This implies the same $G_{bT}$ along the day, what is really extreme. Fig. 3 shows the results. The data corresponds to a really shallow liquid depth $h_l = 5$ mm and a void fraction near to one. Low liquid heights are recommended to minimize the ammonia inventory for safety reasons. For the afternoon parabola orientation, $\gamma_M = 35$ deg, the solar irradiance affects laterally the receiver wall in contact with vapor flow, inducing a local moderate overheating of 35 K and increasing the difference of maximum to minimum temperature from 14 K to 53 K. One has to note the displacement of the high temperature peak down the liquid flow angles owing to heat conduction. These temperature increases will not happen so intensively with a Fresnel collector neither with a higher liquid height $h_l$.

Fig. 4 shows the effect of varying the mirror aperture angle $\alpha_M$ around the base case $\alpha_M = 120$ deg and sun tracking angle measured from zenith (asymmetry) $\gamma_M = 35$ deg in order to show the effect of sun radiance concentration on one side on the temperature side peak. Decreasing the aperture angle $\alpha_M$ reduces wall temperatures below 420 K as a result of a concentration reduction, so that thermal stresses and tube deformations diminish. Increasing the aperture angle causes a higher displacement of the high temperature arch toward either the liquid or the vapor arches, and vice versa, with respect to Fig. 3(B). Geometrical sun concentration increases up to 43 as $G_{bT}$ is considered constant irrespective of the changes in these angles.

Fig. 5 shows the effect of increasing the liquid level $h_l$ above the base case, by an increase of the liquid central angle $\phi_l$, indicated in Fig. 2(B) in order to show the effect of liquid convection on the side temperature peak. Velocity of both fluids change as the liquid is falling freely under the sole action of gravity against friction with the wall (Lecuona et al., 2016). The vapor velocity results from the variation in vapor production and the reduction of the cross section. These effects mean a mass flow increase for both phases and a reduction of the void fraction. The results indicate the beneficial effect of a larger liquid angle $\phi_l$ from the point of view of limiting temperature differences in the wall, so that with $h_l = 20$ mm the wall temperature approaches the corresponding phase temperature, irrespective to $\gamma_M$, owing to $\alpha_l$ is much larger and $\alpha_v$. This case is extreme as more than half the tube cross section is filled with liquid and the high counter-flowing vapor velocity will deform the interphase free surface forming waves. Other effects are considered in (Lecuona et al., 2016).

**Tab. 1. Expressions for the temperature distribution along the periphery of the receiver tube wall for Fig. 2.**

| Sector *j* | Specifics | Equations |
|---|---|---|
| I | $\alpha_i = \alpha_l$<br>$T_i = T_l$<br>$S = a_o C$ | **Ia**: $T_{1a}\langle\phi\rangle = T_{C11a}e^{m_1\phi} + T_{C12a}e^{-m_1\phi} + T_{p1}$ |
| | | **Ib**: $T_{1b}\langle\phi\rangle = T_{C11b}e^{m_1(\phi-\phi_4)} + T_{C12b}e^{-m_1(\phi-\phi_4)} + T_{p1}$ |
| | | $m_1^2 = \frac{r_{av}[\alpha_l + \alpha_e(1+w)]}{kw}$; $T_{p1} = \frac{T_l\alpha_l + T_e\alpha_e(1+w) + G_{bT}a_oC(1+w)}{\alpha_l + \alpha_e(1+w)}$ |
| II | $\alpha_i = \alpha_v$<br>$T_i = T_v$<br>$S = a_o C$ | $T_2\langle\phi\rangle = T_{C21}e^{m_2(\phi-\phi_1)} + T_{C22}e^{-m_2(\phi-\phi_1)} + T_{p2}$ |
| | | $m_2^2 = \frac{r_{av}[\alpha_v + \alpha_e(1+w)]}{kw}$; $T_{p2} = \frac{T_v\alpha_v + T_e\alpha_e(1+w) + G_{bT}a_oC(1+w)}{\alpha_v + \alpha_e(1+w)}$ |
| III | $\alpha_i = \alpha_v$<br>$T_i = T_v$<br>$S = a_o$ | $T_3\langle\phi\rangle = T_{C31}e^{m_3(\phi-\phi_2)} + T_{C32}e^{-m_3(\phi-\phi_2)} + T_{p3}$ |
| | | $m_3^2 = \frac{r_{av}[\alpha_v + \alpha_e(1+w)]}{kw}$; $T_{p3} = \frac{T_v\alpha_v + T_e\alpha_e(1+w) + G_{bT}a_o(1+w)}{\alpha_v + \alpha_e(1+w)}$ |
| IV | $\alpha_i = \alpha_l$<br>$T_i = T_l$<br>$S = a_0$ | $T_4\langle\phi\rangle = T_{C41}e^{m_4(\phi-\phi_3)} + T_{C42}e^{-m_4(\phi-\phi_3)} + T_{p4}$ |
| | | $m_4^2 = \frac{r_{av}[\alpha_l + \alpha_e(1+w)]}{kw}$; $T_{p4} = \frac{T_l\alpha_l + T_e\alpha_e(1+w) + G_{bT}a_o(1+w)}{\alpha_l + \alpha_e(1+w)}$ |

**Tab. 2. Development of the boundary conditions to determine the characteristic temperatures, Fig. 2. Exponents < $2\pi$.**

| | | |
|---|---|---|
| $\boldsymbol{\phi_d = 2\pi}$ | $T_{1b} = T_{1a}$ | $T_{C11b}e^{m_1(\phi_d-\phi_4)} + T_{C11b}e^{-m_1(\phi_d-\phi_4)} + T_{p1} = T_{C11a} + T_{C12a} + T_{p1}$ |
| | $\frac{dT_{1b}}{d\phi} = \frac{dT_{1a}}{d\phi}$ | $m_1T_{C11b}e^{m_1(\phi_d-\phi_4)} - m_1T_{C11b}e^{-m_1(\phi_d-\phi_4)} = m_1T_{C11a} - m_1T_{C12a}$ |

| | | |
|---|---|---|
| $\boldsymbol{\phi = \phi_1}$ | $T_{1a} = T_2$ | $T_{C11a}e^{m_1\phi_1} + T_{C12a}e^{-m_1\phi_1} + T_{p1} = T_{C21} + T_{C22} + T_{p2}$ |
| | $\frac{\mathrm{d}T_{1a}}{\mathrm{d}\phi} = \frac{\mathrm{d}T_2}{d\phi}$ | $m_1 T_{C11a}e^{m_1\phi_1} - m_1 T_{C12a}e^{-m_1*\phi_1} = m_2 T_{C21} - m_2 T_{C22}$ |
| $\boldsymbol{\phi = \phi_2}$ | $T_2 = T_3$ | $T_{C21}e^{m_2(\phi_2-\phi_1)} + T_{C22}e^{-m_2(\phi_2-\phi_1)} + T_{p2} = T_{C31} + T_{C32} + T_{p3}$ |
| | $\frac{\mathrm{d}T_2}{\mathrm{d}\phi} = \frac{\mathrm{d}T_3}{\mathrm{d}\phi}$ | $m_2 T_{C21}e^{m_2(\phi_2-\phi_1)} - m_2 T_{C22}e^{-m_2(\phi_2-\phi_1)} = m_3 T_{C31} - m_3 T_{C32}$ |
| $\boldsymbol{\phi = \phi_3}$ | $T_3 = T_4$ | $T_{C31}e^{m_3(\phi_3-\phi_2)} + T_{C32}e^{-m_3(\phi_3-\phi_2)} + T_{p3} = T_{C41} + T_{C42} + T_{p4}$ |
| | $\frac{\mathrm{d}T_3}{\mathrm{d}\phi} = \frac{\mathrm{d}T_4}{\mathrm{d}\phi}$ | $m_3 T_{C31}e^{m_3(\phi_3-\phi_2)} - m_3 T_{C32}e^{-m_3(\phi_3-\phi_2)} = m_4 T_{C41} - m_4 T_{C42}$ |
| $\boldsymbol{\phi = \phi_4}$ | $T_4 = T_{1b}$ | $T_{C41}e^{m_4(\phi_4-\phi_3)} + T_{C42}e^{-m_4(\phi_d-\phi_3)} + T_{p4} = T_{C11b} + T_{C12b} + T_{p1}$ |
| | $\frac{\mathrm{d}T_4}{\mathrm{d}\phi} = \frac{\mathrm{d}T_{1b}}{\mathrm{d}\phi}$ | $m_4 T_{C41}e^{m_4(\phi_d-\phi_3)} - m_4 T_{C42}e^{-m_4(\phi_d-\phi_3)} = m_1 T_{C11b} - m_1 T_{C12b}$ |

**Tab. 3: Base parameters for the simulations.**

| Tube parameters | Flow parameters ($_l$ liquid, $_v$ vapor) | Solar parameters |
|---|---|---|
| $r_{av}$ = 17.5 mm; $t$ = 1.5 mm; $k$ = 18.5 W K$^{-1}$ m$^{-1}$. $\phi_1$ = 44.4 deg. | $\alpha_l$ = 2,080 W K$^{-1}$ m$^{-2}$;$\alpha_v$ = 100 W K$^{-1}$ m$^{-2}$; $\alpha_e$ = 15 W K$^{-1}$ m$^{-2}$; $h_l$ = 5 mm $T_l$ = 377 K; $T_v$ = 400 K; $T_e$ = 287 K | $G_{bT}$= 817 W m$^{-2}$; $S$ = 21; $\alpha_M$ = 120 deg; $a_0$ = 0.7 |

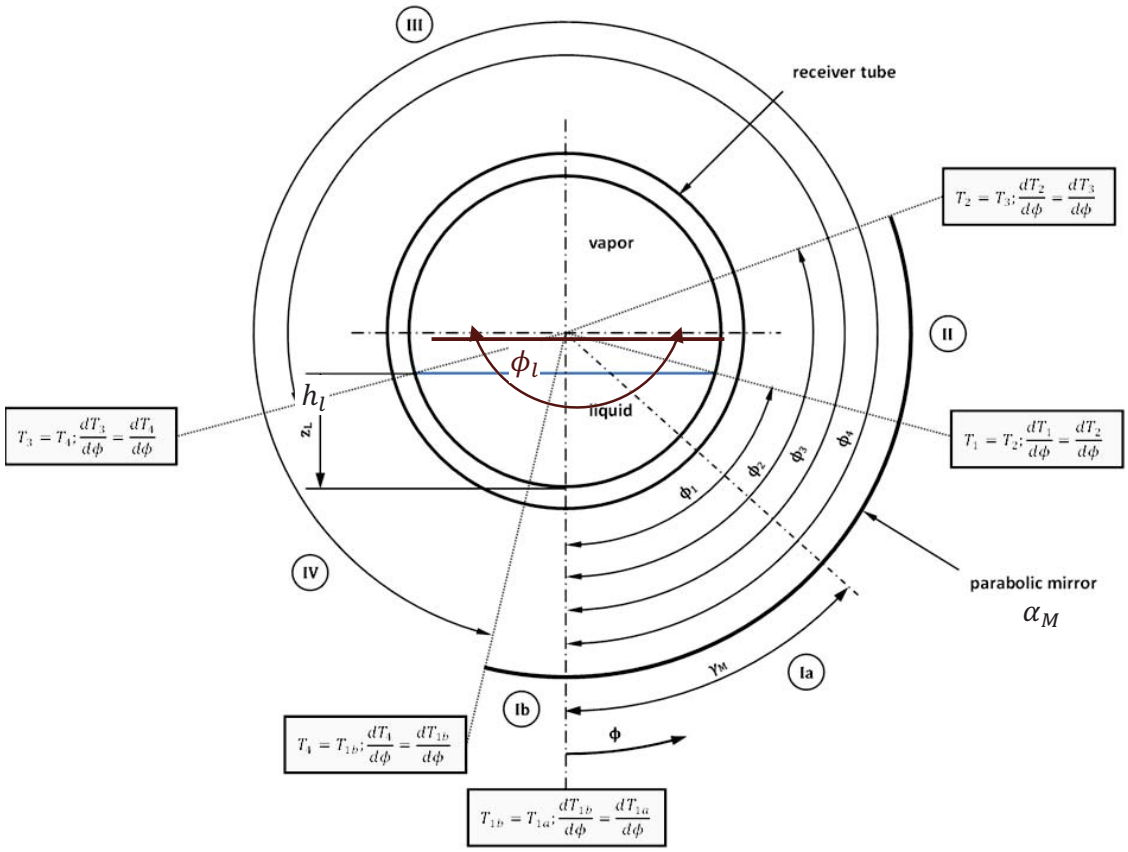


**Fig. 2: Scheme of the peripheral thermal layout and boundary conditions for a parabolic trough, not to scale. $\gamma_M$ represents the sun tracking angle. $h_l$ represents the liquid flow depth.**

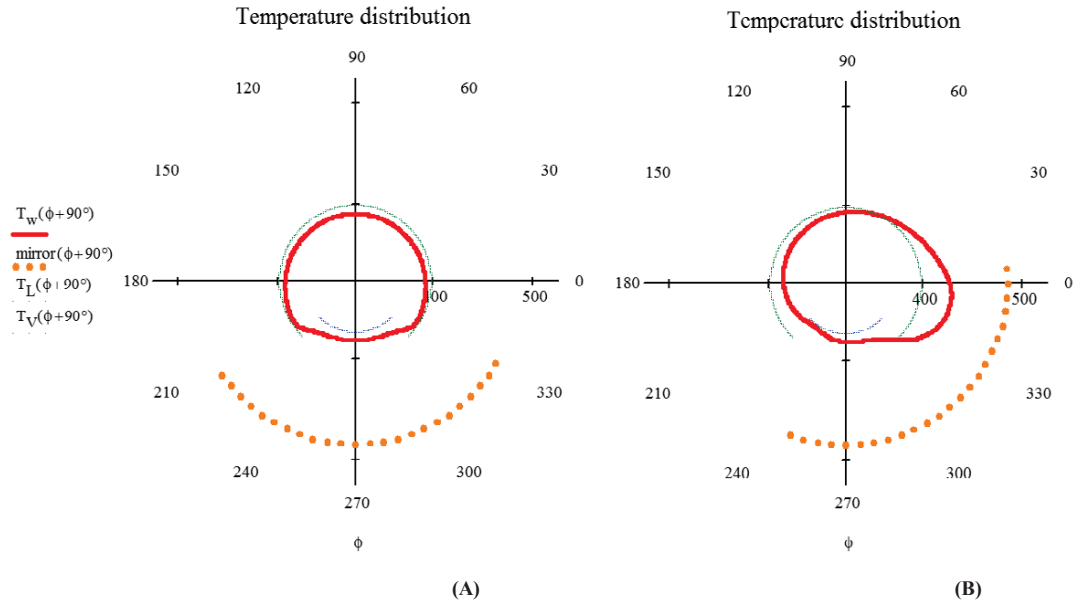


**Fig. 3: Temperatures of the wall as a continuous red line, liquid temperature as continuous violet line and vapor temperature as a continuous green line [K] versus central angle $\phi$ [deg]. Yellow dots represent the aperture angle $\alpha_M = 120$ deg of the parabolic trough mirror. Sun tracking angle A) $\gamma_M = 0$, base case. B) $\gamma_M = 35$ deg, ceteris paribus.**

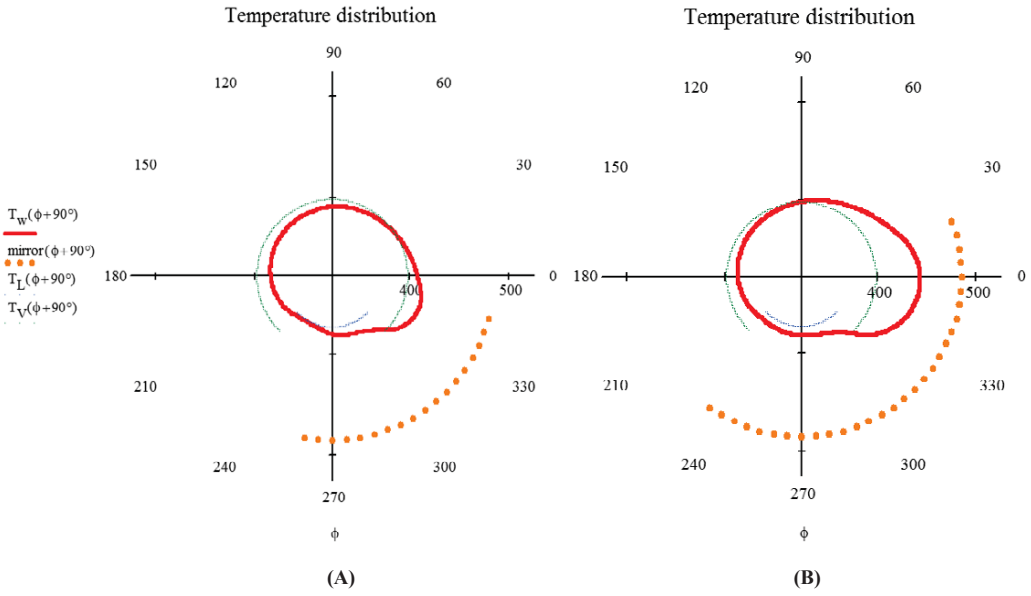


**Fig. 4: Temperatures of the wall as a continuous red line, liquid temperature as continuous violet line and vapor temperature as a continuous green line [K] versus angle $\phi$ [deg]. Yellow dots represent the aperture angle of the parabolic trough mirror. Sun tracking angle $\gamma_M = 35$ deg. A) $\alpha_M = 90$ deg; B) $\alpha_M = 150$ deg, ceteris paribus.**

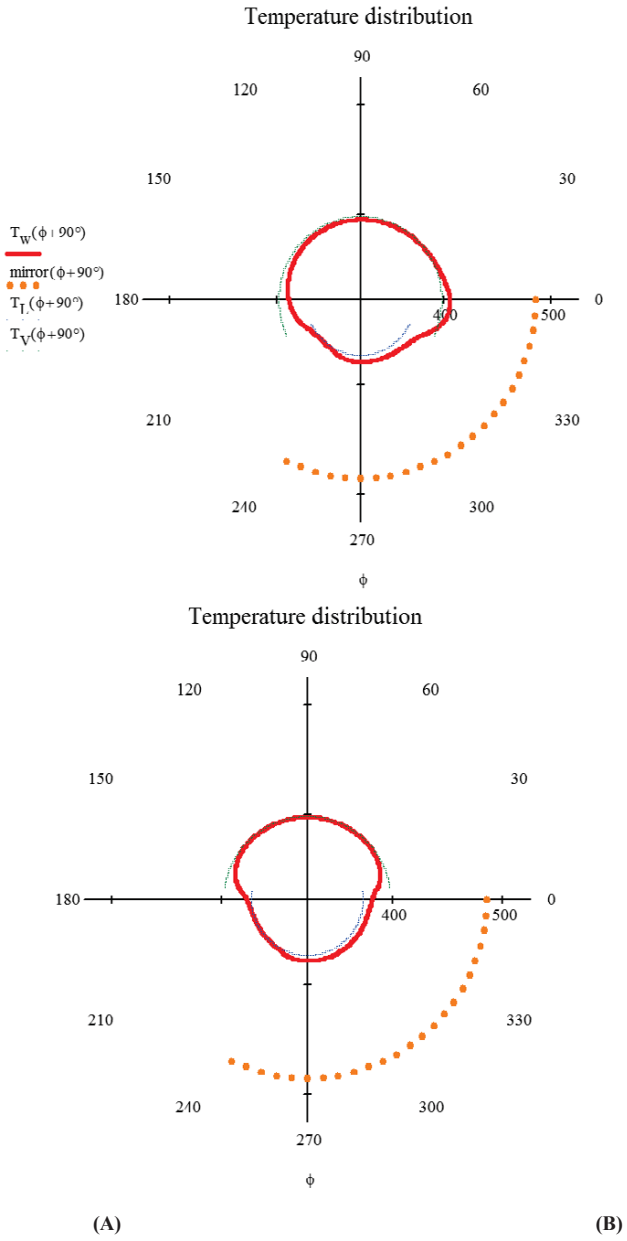


**Fig. 5: Temperatures of the wall as a continuous red line, liquid temperature as continuous violet line and vapor temperature as a continuous green line [K] versus angle $\phi$ [deg]. Yellow dots represent the aperture angle $\alpha_M = 120$ deg of the parabolic trough mirror. Sun tracking angle $\gamma_M = 35$ deg. A) $h_l = 10$ mm; B) $h_l = 20$ mm, ceteris paribus.**

## 4. Conclusions

A simplified method has been developed to estimate the wall temperature peripheral distribution on the circular section of the receiver tube of linear solar collectors, typically of the parabolic trough and Fresnel types. The more complex layout of a vertically gravity stratified counter-current two-phase flow has been studied.

This method relies on an exact solution of the 1D conduction heat transfer, thus more precise than its discretization on finite 1D elements.

The application has been performed to data from a representative medium temperature (MT) parabolic trough collector as it can present the most noticeable temperature inhomogeneities. Results indicate that the

temperature differences can be of concern when either/both the liquid phase central angle $\phi_l$ is small compared with the mirror aperture angle $\alpha_M$. This is more pronounced when a parabolic trough type collector points to the sun when it is out of zenith, $\gamma_M \neq 0$. This caveat is of much lower importance for Fresnel collectors, even lower with secondary optics.

Matching the angle of the liquid sector $\phi_l$ to the mirror aperture angle $\alpha_M$ and even setting it with a larger angle benefits the temperature homogeneity of the receiver tube wall. But having a lower liquid angle is of not much concern during the morning and afternoon, as the irradiance $G_{bT}$ decreases going away from midday, just when wall temperature inhomogeneity tends to increase in parabolic trough collectors.

The data obtained allow developing mass and heat transfer simulations of the innovative layout of direct vapor production using stratified two-phase flows with liquid film driven by gravity. This is of relevance for advanced absorption cycles for polygeneration. They allow also to ascertain the bending of the tube to avoid overstressing and touching the glass envelope.

## 5. Acknowledgements

The partial funding of the research project "Tecnologías energéticas térmico-solares y de aprovechamiento de calores residuales a baja y media temperatura integradas en la red eléctrica", ENE2013-45015-R from the Spanish Ministerio de Economía y Competitividad is greatly appreciated.

## 6. References

Ahmed, M. 2014. *Two Dimension Numerical Modeling of Receiver Tube Performance for Concentrated Solar Power Plant*. Energy Procedia, 57, 551 – 560. doi: 10.1016/j.egypro.2014.10.209

Danfoss. 2015. *De los HFC/HCFC al amoníaco en la refrigeración industrial. Una guía breve sobre el cambio al amoníaco.* Danfoss Group Global. Copenhagen: Danfoss A/S. Retrieved November 11, 2015, from www.danfoss.com/IR-tools.

Duffie, J., & Beckman, W., 1980. *Solar Engineering of Thermal Processes 3rd ed.* Hoboken, New Jersey, USA: Wiley.

Eck, M., Steinmann, W.-D., & Rheinländer, J., 2004. Maximum temperature difference in horizontal and tilted absorber pipes with direct steam generation. *Energy, 29*, 665–676. doi:10.1016/S0360-5442(03)00175-0.*Eck, M., Zarza, E., Eickhoff, M., Rheinlander, J., & Valenzuela, L., 2003. Applied research concerning the direct steam generation in parabolic troughs. *Solar Energy, 74*, 341-351. doi:10.1016/S0038-092X(03)00111-7.

Forristal, R., 2003. *Heat Transfer Analysis and Modeling of a Parabolic Trough in Engineering Equation Solver.* Office of Scientific and Technical Information. Oak Ridge: US Department of Energy. Retrieved November 11, 2015, from http://www.ntis.gov/ordering.htm.

Hernández-Magallanes, J., Domínguez-Inzunza, L., González-Urueta, G., Soto, P., Jiménez, G., & Rivera, W., 2014. Experimental assessment of an absorption cooling system operating with the ammonia/lithium nitrate mixture. *Energy, 78*, 685-692. Retrieved from http://dx.doi.org/10.1016/j.energy.2014.10.058.

Herold, K., Radermacher, R., & Klein, S., 1996. *Absorption chillers and Heat Pumps.* New York: CRC Press.

Incropera, F., & DeWitt, D. 199). *Introduction to Heat Transfer* 2nd ed. New York, New York, USA: John Wiley.

ISO/DIS 9806., 2016. *Solar energy. Solar thermal collectors. Test methods.* ISO. Retrieved August 25, 2016, from http://www.iso.org/iso/catalogue_detail.htm?csnumber=67978.

Jradi, M., & Riffat, S., 2012, October. Medium temperature concentrators or solar thermal applications. *International Journal of Low-Carbon Technologies, 0*, 1-11. doi:10.1093/ijlct/cts068.

Kalogirou, S., 2004. Solar thermal collectors and applications. *Progress in Energy and Combustion Science, 30*, 231–295. doi:10.1016/j.pecs.2004.02.001.

Lecuona, A., Ventas, R., Venegas, M., Zacarías, A., & Salgado, R., 2009. Optimum hot water temperature for absorption solar cooling. *Applied Energy, 83*(10), 1806–1814. doi:10.1016/j.solener.2009.06.016.

Lecuona-Neumann, A., Rosner, M., & Ventas-Garzón, R., 2016. Transversal temperature profiles of two-phase stratified flow in the receiver tube of a solar linear concentrator. Simplified analysis. *EUROSON 2016* (p. in press. Palma de Mallorca: ISES.

Logie, W., Asselineau, C., Pye, J., & Coventry, J. (2015). *Temperature and Heat Flux Distributions in Sodium Receiver Tubes*. 2015 Asia Pacific Solar Research Conference, (p. 10). Queensland. Retrieved September 10, 2016, from https://energystoragealliance.com.au/event/asia-pacific-solar-research-conference-2/

Lobón, D., Valenzuela, L., & Baglietto, E. (2014). *Modeling the dynamics of the multiphase fluid in the parabolic-trough solar steam generating systems*. Energy Conversion and Management, 78, 393–404. doi:10.1016/j.enconman.2013.10.072

Sigalés, B., 2003. *Transferencia de Calor Técnica* (Vol. I). Barcelona, Barcelona, Spain: Reverté.

Ventas, R., Lecuona, A., Vereda, C., & Legrand, M., 2016. Two-stage double-effect ammonia/lithium nitrate absorption cycle. *Applied Thermal Engineering, 94*, 228–237. Retrieved from http://dx.doi.org/10.1016/j.applthermaleng.2015.10.144.

Ventas, R., Lecuona, A., Zacarías, A., & Venegas, M., 2010. Ammonia-Lithium Nitrate Absorption Chiller With An Integrated Low-Pressure Compression Booster Cycle For Low Driving Temperatures. *Applied Thermal Engineering, 30*, Volume 30, Iss1351-1359. doi:10.1016/j.applthermaleng.2010.02.022.

Vereda, C., Ventas, R., Lecuona, A., & López, R., 2014. Single-effect absorption refrigeration cycle boosted with an ejector-adiabatic absorber using a single solution pump. *International Journal of Refrigeration, 38*, 22-29. doi:10.1016/j.irefrig.2013.10.010.

Wang, F., Feng, H., Zhao, J., Li, W., Zhang, F., & Liu, R., 2015. Performance assessment of solar assisted absorption heat pump system with parabolic trough collectors. *Energy Procedia, 70*, 529 – 536. doi:10.1016/j.egypro.2015.02.157.

Wu, W., Wang, B., Shi, W., & Li, X., 2014. An overview of ammonia-based absorption chillers and heat pumps. *Renewable and Sustainable Energy Reviews, 31*, 681–707. doi:http://dx.doi.org/10.1016/j.rser.2013.12.021.

Yang, X., Yang, X., Ding, Y., Shao, Y., & Fan, H. (2012). *Numerical simulation study on the heat transfer characteristics of the tube receiver of the solar thermal power tower*. Applied Energy, 90, 142–147. doi:10.1016/j.apenergy.2011.07.006.

Zamora, M., Bourouis, M., Coronas, A., & Vallés, M., 2014. Pre-industrial development and experimental characterization of new air-cooled and water-cooled ammonia/lithium nitrate absorption chillers. *International journal of refrigeration, 45*, 189-197. doi:10.1016/j.ijrefrig.2014.06.005.